Energy & Environmental Science

Energy scavenging from ultra-low temperature gradients

SCHOLARONE™
Manuscripts

ARTICLE

Energy scavenging from ultra-low temperature gradients

Ravi Anant Kishore, *[a] Brent Davis, [a] Jake Greathouse, [a] Austin Hannon, [a] David Kennedy, [a] Alec Millar, [a] Daniel Mittel, [a] Amin Nozariasbmarz, [b] Min Gyu Kang, [a] Han-Byul Kang, [a] Mohan Sanghadasa [c] and Shashank Priya*[a,b]

Thermal energy harvesting from natural resources and waste heat is becoming critical due to ever-increasing environmental concerns. However, so far, available thermal energy harvesting technologies have only been able to generate electricity from large temperature gradients. Here, we report a fundamental breakthrough in low-grade thermal energy harvesting and demonstrate a device based on the thermomagnetic effect that uses ambient conditions as the heat sink and operates from a heat source at temperature as low as 24°C. This concept can convert temperature gradient as low as 2°C into electricity while operating near room temperature. The device is found to exhibit power density (power per unit volume of active material) of 105 μW/cm³ at temperature difference of 2°C, which increases to 465 μW/cm³ at temperature difference of 10°C. Power density increases by 2.5 times in presence of wind with speed of 2.0 m/s. This advancement in thermal energy harvesting technology will have a transformative effect on renewable energy generation and in reducing global warming.

Introduction

Annually, 340 Exajoule (1 EJ =10^{18} J) of energy out of 474 EJ of energy produced from various renewable and non-renewable energy resources is rejected as waste heat.[1] Low-grade waste heat with temperature less than 100°C constitutes more than 60% of total waste heat.[1] In addition to waste heat available from various industrial and household sources, there are natural thermal energy sources, such as hot springs, geothermal heat, and solar heat, whose temperature varies from room temperature to the evaporation temperature of water. Unarguably, low-grade heat, either in the form of waste heat or natural source, represents an extremely promising source of renewable energy, as it is commonly available in our local surroundings. The Carnot efficiency of a low-grade heat recovery engine operating between 100°C and the ambient at 25°C can be calculated to be about 20%. This infers that a cost-effective method to recover low-grade heat would have transformative impact on overall energy scenario.

Traditionally, binary Organic Rankine cycle [2, 3] and Kalina cycle [4] based power plants have been used for electricity generation from the medium-temperature (100-220°C) heat resources. However, as the available temperature difference is reduced, the performance of these power plants deteriorates and at

temperature below 100°C, cycle efficiency reduces to 5-9%.[5] Further, with low-temperature source, traditional heat engines require large heat exchangers,[6] which imposes additional space and material cost, making them economically unviable. Stirling engine is another popular option for low-grade heat recovery. Small Stirling engines have been reported to start at temperature difference as low as 0.5°C[7] and generate power on the order of 0.3–2.5 mW when the temperature difference is 6.5-19°C.[8, 9] Stirling engines, however, employ gas as the working fluid that requires large storage volume and imposes several operational challenges due to diffusion and leakage.[10] A better alternative to capture low-grade heat is through thermal energy harvesting. Energy harvesting provides methodology for generating electricity from environmental energy sources that are freely available. Energy harvesting devices comprising of solar cells [11, 12] and vibration harvesters [13-15] have been widely pursued in literature and recently there has been surge in developing thermal energy harvesters. Various approaches based upon thermoelectrics, pyroelectrics, thermal polymer-muscles, and shape memory alloys are being considered.[16] The thermoelectric generators (TEGs) utilizing the Seebeck effect represent one of the most popular heat recovery technologies.[17, 18] Although recent studies have reported TEG efficiency close to 10% when temperature gradient is large (more than 500°C),[19, 20] efficiency of commercially available TEGs is still quite low, not more than few percent.[21] The efficiency of TEGs, and indeed all heat engines, deteriorates as the thermal gradient decreases, which makes them impractical for low-grade heat recovery (hot-side temperatures lower than 100°C). This is related to peak behaviour of figure-of-merit for thermoelectric materials, which in most cases occurs above 100°C. Shape memory alloy (SMA) based generators have been

recently proposed as an alternative for low temperature heat recovery.[22, 23] SMA engines rely on a thermoelastic effect, where an SMA element undergoes reversible phase transformation from martensite to austenite phase, generating cyclic strain, which is used to generate torque that drives an electromagnetic generator. SMA engines have been reported to operate in the temperature range of 60-80°C and found to exhibit 187 mW of electrical power from a device with dimensions 1850 mm x 550 mm x 500 mm, resulting in power density of 0.4 W/m^3.[22] Pyroelectrics and thermal polymer-muscles have been projected to exhibit high power density (1.08 MW/m^3 of the PVDF film under a temperature change of 80°C for a pyroelectric generator [24] and 18.1 kW/m^3 of the coiled muscle across temperature fluctuation of 70°C for the polymer-muscle powered tensile energy generator)[25]. Although both these technologies are being targeted for waste heat recovery, their requirement of cyclic temperature variation limits their deployment. In addition, high power density in these cases is accompanied by very low overall power output for a given volume, which makes the integration or operation such as recharging of batteries quite difficult.

A fundamentally different approach for harnessing low-grade thermal energy and converting it into mechanical or electrical energy is possible using thermomagnetic effect. The concept of a thermomagnetic generator was first proposed in the late 19th century,[26-29] but this promising technology was not implemented due to lack of a suitable ferromagnetic material. The conventional ferromagnetic materials such as iron, cobalt, and nickel have Curie temperature above 350°C, which presents several implementation challenges. Gadolinium (Gd), having low Curie temperature of 22°C, has been proposed as a suitable thermomagnetic material for a thermomagnetic generator.[30] Ferromagnetic to paramagnetic transition normally occurs in a narrow temperature range; therefore, in comparison with the conventional ferromagnetic materials, Gd is expected to exhibit higher Carnot efficiency for the same value of ΔT (i.e. for a fixed temperature difference, ΔT, Carnot efficiency $\Delta T / T_h$ increases with decease in hot reservoir temperature T_h).[31] Analytical studies [32-35] have revealed that Gd based thermomagnetic heat engines can provide efficiency approaching the Carnot efficiency; however, no known experimental work has been performed to prove this possibility which indicates the challenges associated with translating the theory into practice. Factors such as material availability, manufacturability, actual operating condition, environmental effects, and cost are just the few challenges that often lead to violation in assumptions made in analytical calculation. Few recent studies[36-40] have reported Gd based thermomagnetic harvesters, however, these devices often require a heat sink below 0°C, which questions the economic feasibility of these low power density devices.

In this study, we demonstrate a unique ultra-low thermal gradient energy recovery mechanism, called PoWER (Power from Waste Energy Recovery), with ambient acting as the heat sink. PoWER device does not require an external heat sink, bulky fins or thermal fluid circulation. Small size, room temperature operation, and cost-effective configuration makes our device highly suitable for power generation in a wide range of applications including recharging a battery for internet-of-things, self-powered temperature sensing, water quality monitoring, occupancy detection sensors, and power generation. A PoWER device utilizes the thermomagnetic effect, where cyclic variation in temperature across the Curie temperature of a ferromagnetic material in the presence of an external magnetic field results in cyclic change in magnetization, which is used to create mechanical work. A home built two-rotor one-stator axial flux electric generator is connected to thermomagnetic engine to convert mechanical power into electricity.

Results and discussion

Material, working principle, and device design

The thermomagnetic material employed in this study is Gd as its Curie temperature is close to the room temperature. Gd possess a large magnetic moment below its Curie temperature because of its electronic configuration, [Xe] 4f^7 5d^1 6s^2. Fig. 1a depicts the electronic configuration in the outer orbit of a neutral Gd atom.[41] The seven unpaired electrons in its 4f subshell account for a total angular momentum (spin angular momentum, S, and orbital angular momentum, L) of $J = L + S = 7/2$.[42] The saturation magnetic moment of Gd has been reported to be $7.55\mu_B$. Additional $0.55\mu_B$ moment is attributed to a conduction electron polarization.[43] Gd crystallizes in the hexagonal close-packed structure and from spin reorientation temperature (-41°C) to Curie temperature (22°C), the magnetic moments are aligned along the hexagonal axis (c-direction), as shown in Fig. 1b.[44]

Gd undergoes the second-order paramagnetic↔ferromagnetic phase transformation, which can be utilized to obtain magnetic work using the thermomagnetic cycle shown in Fig. 1c and d. Phase i, shown in Fig. 1c and d, denotes the state of spontaneous magnetization where a Gd sample is below its Curie temperature and in zero external magnetic field. When external magnetic field H+ is applied, the magnetic moments orient in the direction of magnetic field, leading to increase in the size of magnetic domains (shown as state ii). The Gd sample is then heated above the Curie temperature while the external magnetic field is maintained constant. Magnetization reduces due to thermal agitation, which is indicated by state iii. When the external magnetic field is removed, the magnetic moments fully disorient, leading to near zero magnetization in the Gd sample (state iv). Lastly, the Gd sample is cooled to its initial temperature and state i is restored. It is important to note that when the temperature across a ferromagnetic material is changed, the material needs some time to establish a new equilibrium magnetization. This characteristic time is termed as the spin-lattice relaxation time and it measures the strength of the coupling between the spin system and the lattice. In case of Gd, the characteristic time for establishing thermal equilibrium

between the lattice and the spin system has been reported to be on the order of picoseconds.[45] Since the magnetic response of Gd is quite fast, the overall frequency of a Gd-based thermomagnetic cycle is primarily controlled by the frequency at which thermal cycling occurs.

Fig. 1e demonstrates the working principle of the proposed PoWER mechanism based on thermomagnetic effect. The PoWER device consists of ring-shaped Gd rotors, permanent magnets, and an electric generator. Fig. 1f shows an assembled PoWER device having six rotors. Warm water ($T_h = $ 24-50°C) is used as the hot reservoir to heat a small section of the Gd rotor above its Curie temperature. The external magnetic field is created using the two permanent magnets located in opposite polarity below the rotors. This two-magnet configuration helps the PoWER device to achieve higher rotor speed and magnetic torque as compared to the one-magnet configuration (please refer ESI Fig. S6 for more discussion). The portion of the rotor in contact with the warm water gains heat and a hot spot is created. When temperature rises above the Curie temperature, the rotor locally undergoes second-order ferromagnetic to paramagnetic phase transformation, causing the magnetic domains to disorient due to thermal agitation. This drastically reduces the magnetic interaction between the hot spot and the permanent magnet. Since the remaining part of the rotor is still cold and in ferromagnetic phase, the permanent magnet attracts a cooler portion resulting in a net torque on the rotor, which causes it to rotate. As rotation occurs, the hot portion cools down by dissipating heat to the ambient and the magnetic domains regain their orientation. Eventually, a new hot spot is created, and the rotation continues as long as there is a heat source. An axial flux electric generator is connected to the rotor in order to harvest this rotational motion and generate electricity. The details on the device fabrication is provided in the experimental section. A detailed discussion on thermomagnetic effect, thermomagnetic material, and the calculation for specific work and efficiency of thermomagnetic cycle are provided in the ESI.

Thermomagnetic cycle in the PoWER rotor

Fig. 2a-b illustrates the magnetic field distribution and temperature distribution along the rotor's surface of the PoWER device. The contours were obtained using COMSOL Multiphysics (version 5.3). As shown in Fig. 2a, the magnetic flux density varies between ~0 T and 0.22 T. This infers that during each rotation, a portion of the rotor experiences a magnetic cycle in the range 0-0.22 T. Fig. 2b shows the temperature contour. It was noted that the actual temperature distribution is dependent on the rotor's angular speed; however, the extreme values for rotor temperature always lie between the water and ambient temperature. Fig. 2c depicts the magnetization versus magnetic field (M-H) plots for Gd, obtained using the quantum design physical property measurement system (PPMS). Using Equation (S1) and integrating around the thermomagnetic cycle, the specific magnetic work per thermomagnetic cycle occurring between 0-0.22 T and 22-40°C can be calculated to be ~3.5 J/kg. In Fig. 2c,

it is also important to note that the isotherms are very close when temperature is greater than 40°C. This implies that the performance of PoWER devices cannot be increased substantially by increasing the hot-side temperature beyond 40°C. Fig. 2d shows the specific heat versus temperature (C_H-T) plots for Gd measured using differential scanning calorimetry (DSC). The shaded region depicts the heat flow when temperature cycle occurs between 22°C and 40°C. Using Equation (S8), the efficiency of the thermomagnetic cycle was calculated to be ~0.1%. Since, the specific work output per thermomagnetic cycle increases with increase in the applied magnetic field, it is estimated that when applied magnetic field is 1.0 T, the efficiency can be increased to 0.6%. Please note that the Carnot efficiency of a heat engine working between $T_c = $ 22°C and $T_h = 40°C$ is 5.8%. This illustrates that thermomagnetic cycle based PoWER devices have potential to operate up to 10% of Carnot efficiency.

Performance characteristic of the PoWER devices

Fig. 3a depicts electrical power produced by the PoWER device having a single rotor of dimension of 50.5 mm (outer diameter, OD) x 44.5 (inner diameter, ID) x 1.5 mm (thickness), when warm water temperature is maintained at 40°C and ambient temperature is at 22°C. The maximum, minimum, and average electrical power obtained during experiments are shown in Fig. 3a at different resistive loads. The maximum average electrical power of 0.385 mW was obtained at the optimal resistive load of 3 kΩ. Fig. 3b depicts electrical power produced by the PoWER device with a rotor of same OD and ID as discussed earlier but different thickness of 3.18 mm. The maximum average electrical power of 0.407 mW was observed at the optimal resistive load of 4 kΩ. This indicates that there is not much gain in power by increasing the rotor thickness, but this is an important result that illustrates the role of coupling between thermal transport and physical behavior of the material. Gd, the thermomagnetic material used for the rotor, has low thermal conductivity of 9.5 W/m-K.[46] Analytical calculations show that heat propagates just few microns inside the rotor when it is operating at the optimal load in the steady state condition. The thermal cycling, therefore, occurs only near the outer surface, making the additional thickness unnecessary. ESI Fig. S4 depicts the effect of size of the rotor on performance of the PoWER devices. It can be noted that increasing the size of the rotor has positive influence on the generated electrical power due to increased thermal gradient. Therefore, in the remainder of paper, results on rotor of dimension 50.0 mm (OD) x 44.5 (ID) x 1.5 mm (thickness) will be presented. Fig. 3c depicts the angular speed progression of the PoWER rotors (not connected to a generator) from the time it starts and until it reaches the steady state. It can be noted that increasing the number of rotors does not significantly affect the steady state angular speed and the rate of angular acceleration; although the maximum angular speed has slightly decreased after three rotors due to an additional damping. This indicates that the thermomagnetic cycle

occurring in different rotors are mutually independent of each other and the magnetic torque can be increased by multiplying the number of rotors. Fig. 3d shows open circuit (OC) voltage produced by the PoWER device having variable number of rotors (one to six), connected simultaneously to a single generator shaft. In order to account for the increased magnetic torque due to multiple rotors, a bigger electric generator compared to the generator used for the PoWER device with a single rotor was implemented. The details on generator characteristics are provided in ESI. The EMF frequency of the electric generator is related to the shaft rpm by relation: $f = np/120$, where n is shaft rpm and p denotes number of magnetic pole pairs used in the electric generator. The steady state, no-load rpm for PoWER devices having one, two, four, and six rotors was found to be 191, 196, 202, and 215, respectively at water temperature of 40°C. This corresponds to operational frequency of 12.7 Hz, 13.1 Hz, 13.5 Hz, and 14.3 Hz, respectively where OC voltages were measured. The output voltage amplitude above 1.0 V ensures minimal losses during AC to DC rectification.

Fig. 4a and b depict the electrical power produced by the PoWER device having multiple rotors, connected simultaneously to a single generator shaft. It can be observed that at hot water temperature of 32°C, the electrical power at the optimal resistive load increases from 0.31 mW to 1.10 mW by increasing the number of rotors from one to six. Likewise, at hot water temperature of 40°C, the optimal electrical power increases from 0.30 mW to 1.30 mW by increasing the number of rotors from one to six. As indicated in Fig. 4c, the optimal power of the PoWER device increases almost linearly with increase in the number of rotors. Fig. 4d shows the output power of the PoWER device with six rotors at different hot-water temperature. It is interesting to note that the PoWER device operates at water temperature of 24°C (i.e. temperature difference of just 2°C) and produces electrical power of 0.42 mW, which increases to 0.79 mW at water temperature of 27°C (temperature difference of 5°C), 1.10 mW at water temperature of 32°C (temperature difference of 10°C), and 1.30 mW at water temperature of 40°C (temperature difference of 18°C). More detailed discussion on scalability of PoWER devices is provided in ESI.

PoWER device performance as a function of temperature

Fig. 5a and b demonstrate the performance of the PoWER device with three rotors during a temperature sweep experiment. As indicated in Fig. 5a, the rotor rpm initially increases with increase in water temperature, but then saturates at ~50°C. This happens because of the counteractive effects between thermal and magnetic physics. The convective heat transfer coefficient is proportional to relative speed between the ambient air and the rotating rotor, whereas the magnetic force is proportional to the lowest temperature achieved by the rotor. When water temperature is low, the

rotor tends to move faster as a higher rpm helps the hot spot in the rotor to cool faster and thus amplifies the paramagnetic to ferromagnetic phase transformation. However, when temperature of the hot spot is much above the Curie point, the high rpm of the rotor does not allow it to cool below the Curie temperature, thereby restricting paramagnetic to ferromagnetic phase transition. Therefore, when water temperature is low (25-30°C), the rotor speeds up, however when water temperature rises to a threshold value of ~50°C, the rotor attains constant speed of around 200 rpm. Similar trend was observed for power output (Fig. 5b). The electrical power of the PoWER device first increases with increase in temperature, reaches a maximum value at 35-45°C, then decreases slowly. This can be explained by invoking the M-H diagram shown in Fig. 2c. Since the isotherms are close at high temperature, the shaded area does not increase substantially beyond 40°C, thereby causing a very small increase in the power generated by PoWER devices. The temperature sweep experiments were repeated on the PoWER device with two rotors, which are shown in Fig. S2 and S3 in ESI.

Effect of wind on the performance of PoWER devices

Fig. 6a-d quantify the effect of wind (forced cooling) on the performance of the PoWER devices. The optimal power of the PoWER device with three rotors increases from 0.69 mW under no wind conditions to 1.5 mW under wind speed of 1.5 m/s and to 1.8 mW under wind speed of 2.0 m/s. Likewise, the optimal power of a PoWER device with six rotors increases from 1.3 mW under no wind conditions to 2.3 mW under wind speed of 1.5 m/s and to 2.8 mW under wind speed of 2.0 m/s. Fig. 6c depicts an interesting behavior from a PoWER device. It was observed that the PoWER device is capable of operating with no heat source when there is light wind. As shown in ESI Video V1, the PoWER device does not self-start when there is no heat source; however, once it is started manually, the rotor maintains oscillation. The chilling effect produced by the wind evaporates water drawn on the exposed portion of the rotor during oscillations. This causes the exposed portion of the rotor to cool slightly below the room temperature, thereby creating a thermal gradient in the rotor. The continuous rewetting of the Gd rotor and evaporation by the wind allows the PoWER device to maintain oscillation. The axial AC generator, which is attached to the rotor, captures this oscillation and generates electricity. Fig. 6d shows the voltage across the two terminals of a 2.5 V 0.2 F capacitor, which was charged using the power produced by the PoWER device under wind of 2.0 m/s and no heat source.

Power density of the PoWER devices

Fig. 7 shows the power density (power per unit volume of Gd) of the PoWER devices at two different temperatures. At a fixed temperature difference of 10°C, the power density of 467 $\mu W/cm^3$ is obtained with single rotor. As the number of rotors

is increased, the power density slowly decreases and almost saturates at 265 μW/cm^3 for six rotors. Likewise, at a fixed temperature difference of 18°C, the power density of 442 μW/cm^3 is obtained with two rotors and as the number of rotors is increased, the power density decreases and it approximately saturates at 328 μW/cm^3 for six rotors. Figure in the inset shows power density for the PoWER device with six rotors under varying temperature difference. The PoWER device with six rotors produces power density of 105 μW/cm^3 under temperature difference of 2°C, which increases to 328 μW/cm^3 under temperature difference of 18°C.

There are limited number of studies in the literature that quantify experimental output power for a heat engine operating near room temperature under such low temperature gradients. Most of the thermomagnetic harvesters reported in the literature are based on the linear oscillation of a thermomagnetic material attached to a spring-mass system. They also rely on the piezoelectric effect to generate electricity.[36-39, 47] Based on the average power reported by Chen et al.,[38] the power density (power per unit volume of the thermomagnetic material) of such harvesters was estimated to be 0.0132 μW/cm^3 at temperature difference of 20°C, which is lower by several orders of magnitude than the power density demonstrated by PoWER devices. It is also important to note that the current version of PoWER devices utilizes commercial off-the-shelf non-optimized thermomagnetic material, Gd. There are several prototype thermomagnetic materials, such as GdSiGe alloys[48, 49] and Heusler alloys,[50, 51] that have been reported to exhibit 2-10 times higher thermomagnetic effect than that of Gd. In addition, simulation results shown in ESI shows that performance of the PoWER devices can be increased by increasing the applied magnetic field. This implies that the power density of PoWER devices can be improved by several folds by performing material and system optimization in future studies. We believe PoWER will provide the foundation to launch new generation of thermal energy harvesting devices.

Real-world demonstrations using PoWER devices

Fig. 8a-d demonstrate the deployment of PoWER devices for real-world applications. In Fig. 8a, the PoWER device with a single rotor was kept on the surface of a laptop. Gaining the heat dissipated by the laptop, water temperature below the rotor rises to 25°C, when the room temperature is at 22°C. As shown in ESI Video V2, under temperature difference of just 3°C, PoWER device with single rotor can be seen to light up several LEDs. Fig. 8b demonstrates the operation of the PoWER device when it is located on sewer grill. The demonstration shown in ESI Video V3 depicts that PoWER device can be employed to generate electricity using rejected heat from the steam coming out of sewage and drainage system from industrial and commercial establishments. In Fig. 8c, PoWER device with single rotor is kept on a metal bench, which is exposed to sun light. ESI Video V4 shows the demonstration, where PoWER device can be seen to operate under thermal

gradient of just 1°C (ambient temperature is 25.3°C, whereas the water temperature is 26.3°C). PoWER device was also employed to continuously run MIDASCON wireless sensor that senses temperature, humidity, and acceleration and transmits the data using Bluetooth, as shown in Fig. 8d and ESI Video V5. These successful demonstrations clearly indicate that PoWER device can harvest thermal energy from variety of heat sources and can be used in a wide range of applications.

Conclusions

We report a fundamental breakthrough in demonstrating an ultra-low grade thermal energy recovery mechanism, termed as PoWER (Power from Wasted Energy Recovery), based on the thermomagnetic effect. The PoWER device uses ambient as the heat sink and is found to operate with a heat source at temperature as low as 24°C. The PoWER device is found to exhibit power density (power per unit volume of Gd) of 105 μW/cm^3 at temperature difference of 2°C, which increased to 465 μW/cm^3 at temperature difference of 10°C. Power density increases by 2.5 times in presence of light wind with speed of 2.0 m/s. The PoWER device is also able to operate at zero thermal gradient when there is light wind.

Experimental

Fabrication of PoWER devices

In order to demonstrate the PoWER mechanism, we fabricated the scaled versions of the PoWER device. The device consists of Gd ring shaped rotors of outer diameter (OD) 50.5 mm and inner diameter (ID) 44.5 mm, permanent magnets of size 12.7 mm x 6.35 mm x 6.35 mm, and an axial flux generator. Preliminary experiments reveal that two permanent magnets located in opposite polarity below the rotor provide the highest power (effect of number of permanent magnets on the performance of PoWER device is discussed in ESI). Gd sheets (purity: 99.9%) of 200 mm x 400 mm x 1.5 mm purchased from Stanford Advanced Materials, Inc., USA were used to fabricate rotors for the PoWER devices. Nickel-plated neodymium block magnets of dimension 12.7 mm x 6.35 mm x 6.35 mm were purchased from K&J magnetics, Inc., USA. These permanent magnets were magnetized through their thickness and had a surface field strength of 5248 Gauss. An axial flux generator was built as it has low cogging torque. The details on the generator developed in this study are provided in ESI. As shown in ESI Fig. S4, the axial flux electric generator used in the PoWER device had one stator and two rotors on either sides of the stator. The stator consists of a set of eight teardrop shaped coils; each coil has copper wire of gauge size 42 AWG. Each of the generator rotors contains a set of eight arc shaped permanent magnets. All other components were 3D printed.

Measurement of electrical output and characteristics

Voltage generated by the PoWER devices was recorded using National Instrument's NI myDAQ. The angular speed was

measured using non-contact type optical, digital Tachometer, DT-209X by SHIMPO Instruments, USA. A resistance substitution box, RS-200W, by IET Labs, Inc. was used during resistance sweep experiment. Type T thermocouples were used to detect the temperature of the heat source. For calculating the electrical power, we have used root mean square (rms) voltage. We first recorded the continuous data for rms voltage, which was obtained using consecutive data points for instantaneous voltage. The arithmetic mean of the recorded rms voltage data was then used to calculate the average power, which is reported in Fig. 4a-d and Fig. 6a-b. The maximum and minimum values of the power shown in Fig. 3a-c were calculated based on maximum rms voltage and minimum rms voltage recorded during the resistance sweep experiments. Effect of wind on the performance of the PoWER devices was studied using the 0.7 m subsonic open jet wind tunnel. The magnetic characterization of the Gd sample was performed using the quantum design physical property measurement system (PPMS). The specific heat measurement was performed using differential scanning calorimetry (DSC).

Author contributions

R.A.K. and S.P. conceived the idea; B.D. and J.G. fabricated electric generator; R.A.K, D.K., A.H., and A.M. performed the experiments; R.A.K., D.K and D.M. prepared the demonstration videos. M.G.K and H.K. performed the magnetic characterization. A.N. performed the DSC measurements. S.P. supervised the research. All authors contributed to the discussion. R.A.K and S.P. wrote the manuscript.

Conflicts of interest

There are no conflicts to declare.

Acknowledgements

References

1. C. Forman, I. K. Muritala, R. Pardemann and B. Meyer, *Renewable and Sustainable Energy Reviews*, 2016, **57**, 1568-1579.

2. B.-T. Liu, K.-H. Chien and C.-C. Wang, *Energy*, 2004, **29**, 1207-1217.

3. B. Mohanty and G. Paloso, *Heat Recovery Systems and CHP*, 1992, **12**, 143-158.

4. A. Kalina and H. Leibowitz, *Trans.-Geotherm. Resour. Counc*, 1989, **13**, 605-611.

5. E. Barbier, *Renewable and Sustainable Energy Reviews*, 2002, **6**, 3-65.

6. H. M. Hettiarachchi, M. Golubovic, W. M. Worek and Y. Ikegami, *Energy*, 2007, **32**, 1698-1706.

7. J. Senft, *Mechanical efficiency considerations in the design of an ultra low temperature differential Stirling engine*, Report 0148-7191, SAE Technical Paper, 1992.

8. M. Y. Won and P. S. Jung, *Transactions of the Korean Society of Mechanical Engineers B*, 2005, **29**, 519-525.

9. K. Wang, S. R. Sanders, S. Dubey, F. H. Choo and F. Duan, *Renewable and Sustainable Energy Reviews*, 2016, **62**, 89-108.

10. D. Thimsen, *EPRI, Palo Alto*, 2002, **1007317**.

11. B. J. Kim, D. H. Kim, Y.-Y. Lee, H.-W. Shin, G. S. Han, J. S. Hong, K. Mahmood, T. K. Ahn, Y.-C. Joo and K. S. Hong, *Energy & Environmental Science*, 2015, **8**, 916-921.

12. J. Yoon, A. J. Baca, S.-I. Park, P. Elvikis, J. B. GEDDES III, L. Li, R. H. Kim, J. Xiao, S. Wang and T.-H. Kim, in *Materials for Sustainable Energy: A Collection of Peer-Reviewed Research and Review Articles from Nature Publishing Group*, World Scientific, 2011, pp. 38-46.

13. M.-L. Seol, J.-H. Woo, S.-B. Jeon, D. Kim, S.-J. Park, J. Hur and Y.-K. Choi, *Nano Energy*, 2015, **14**, 201-208.

14. Z. L. Wang, J. Chen and L. Lin, *Energy & Environmental Science*, 2015, **8**, 2250-2282.

15. G. T. Hwang, M. Byun, C. K. Jeong and K. J. Lee, *Advanced healthcare materials*, 2015, **4**, 646-658.

16. R. Kishore and S. Priya, *Materials*, 2018, **11**, 1433.

17.   S. J. Kim, H. E. Lee, H. Choi, Y. Kim, J. H. We, J. S. Shin, K. J. Lee and B. J. Cho, *ACS nano*, 2016, **10**, 10851-10857.

18.   S. J. Kim, H. Choi, Y. Kim, J. H. We, J. S. Shin, H. E. Lee, M.-W. Oh, K. J. Lee and B. J. Cho, *Nano energy*, 2017, **31**, 258-263.

19.   X. Hu, P. Jood, M. Ohta, M. Kunii, K. Nagase, H. Nishiate, M. G. Kanatzidis and A. Yamamoto, *Energy & Environmental Science*, 2016, **9**, 517-529.

20.   A. Muto, J. Yang, B. Poudel, Z. Ren and G. Chen, *Advanced Energy Materials*, 2013, **3**, 245-251.

21.   C. B. Vining, *Nature materials*, 2009, **8**, 83-85.

22.   Y. Sato, N. Yoshida, Y. Tanabe, H. Fujita and N. Ooiwa, *Electrical Engineering in Japan*, 2008, **165**, 8-15.

23.   D. Avirovik, R. A. Kishore, D. Vuckovic and S. Priya, *Energy Harvesting and Systems*, 2014, **1**, 13-18.

24.   Q. Leng, L. Chen, H. Guo, J. Liu, G. Liu, C. Hu and Y. Xi, *Journal of Materials Chemistry A*, 2014, **2**, 11940-11947.

25.   S. H. Kim, M. D. Lima, M. E. Kozlov, C. S. Haines, G. M. Spinks, S. Aziz, C. Choi, H. J. Sim, X. Wang and H. Lu, *Energy & Environmental Science*, 2015, **8**, 3336-3344.

26.   T. A. Edison, *US Pat., 380100*, 1888.

27.   T. A. Edison, *US Pat., 476983*, 1892.

28.   N. Tesla, *US Pat., 396121*, 1889.

29.   N. Tesla, *US Pat., 428057*, 1890.

30.   J. Elliott, *Journal of Applied Physics*, 1959, **30**, 1774-1777.

31.   R. A. Kishore and S. Priya, *Renewable and Sustainable Energy Reviews*, 2018, **81**, 33-44.

32.   L. D. Kirol and J. I. Mills, *Journal of applied physics*, 1984, **56**, 824-828.

33.   D. Solomon, *Journal of applied physics*, 1988, **63**, 915-921.

34.   D. Solomon, *Journal of Applied Physics*, 1989, **65**, 3687-3693.

35.   D. Solomon, *Energy Conversion and Management*, 1991, **31**, 157-173.

36.   J. Chun, H.-C. Song, M.-G. Kang, H. B. Kang, R. A. Kishore and S. Priya, *Scientific Reports*, 2017, **7**, 41383.

37.   M. Ujihara, G. Carman and D. Lee, *Applied Physics Letters*, 2007, **91**, 093508.

38.   C.-C. Chen, T.-K. Chung, C.-Y. Tseng, C.-F. Hung, P.-C. Yeh and C.-C. Cheng, *IEEE Transactions on Magnetics*, 2015, **51**, 1-9.

39.   L. Carlioz, J. Delamare and S. Basrour, 2009.

40.   J. Chun, R. A. Kishore, P. Kumar, M.-G. Kang, H. B. Kang, M. Sanghadasa and S. Priya, *ACS applied materials & interfaces*, 2018, **10**, 10796-10803.

41.   *Gadolinium: http://mriquestions.com/why-gadolinium.html. Accessed on 12/20/2018.*

42.   S. Y. Dan'Kov, A. Tishin, V. Pecharsky and K. Gschneidner, *Physical Review B*, 1998, **57**, 3478.

43.   J. Cable and E. Wollan, *Physical Review*, 1968, **165**, 733.

44.   M. Rotter, M. Doerr, A. Lindbaum and A. Massalami, 2002.

45.   A. Vaterlaus, T. Beutler and F. Meier, *Physical review letters*, 1991, **67**, 3314.

46.   C. Glorieux, J. Thoen, G. Bednarz, M. A. White and D. Geldart, *Physical Review B*, 1995, **52**, 12770.

47.   H.-C. Song, D. Maurya, J. Chun, Y. Zhou, M.-E. Song, D. Gray, N. K. Yamoah, D. Kumar, A. McDannald and M. Jain, *Energy Harvesting and Systems*, 2017, **4**, 57-65.

48.   V. K. Pecharsky and K. A. Gschneidner Jr, *Applied Physics Letters*, 1997, **70**, 3299-3301.

49.   V. Pecharsky and K. Gschneidner Jr, *Journal of Magnetism and Magnetic Materials*, 1997, **167**, L179-L184.

50.   F.-x. Hu, B.-g. Shen, J.-r. Sun and G.-h. Wu, *Physical Review B*, 2001, **64**, 132412.

51.   F.-x. Hu, B.-g. Shen and J.-r. Sun, *Applied Physics Letters*, 2000, **76**, 3460-3462.
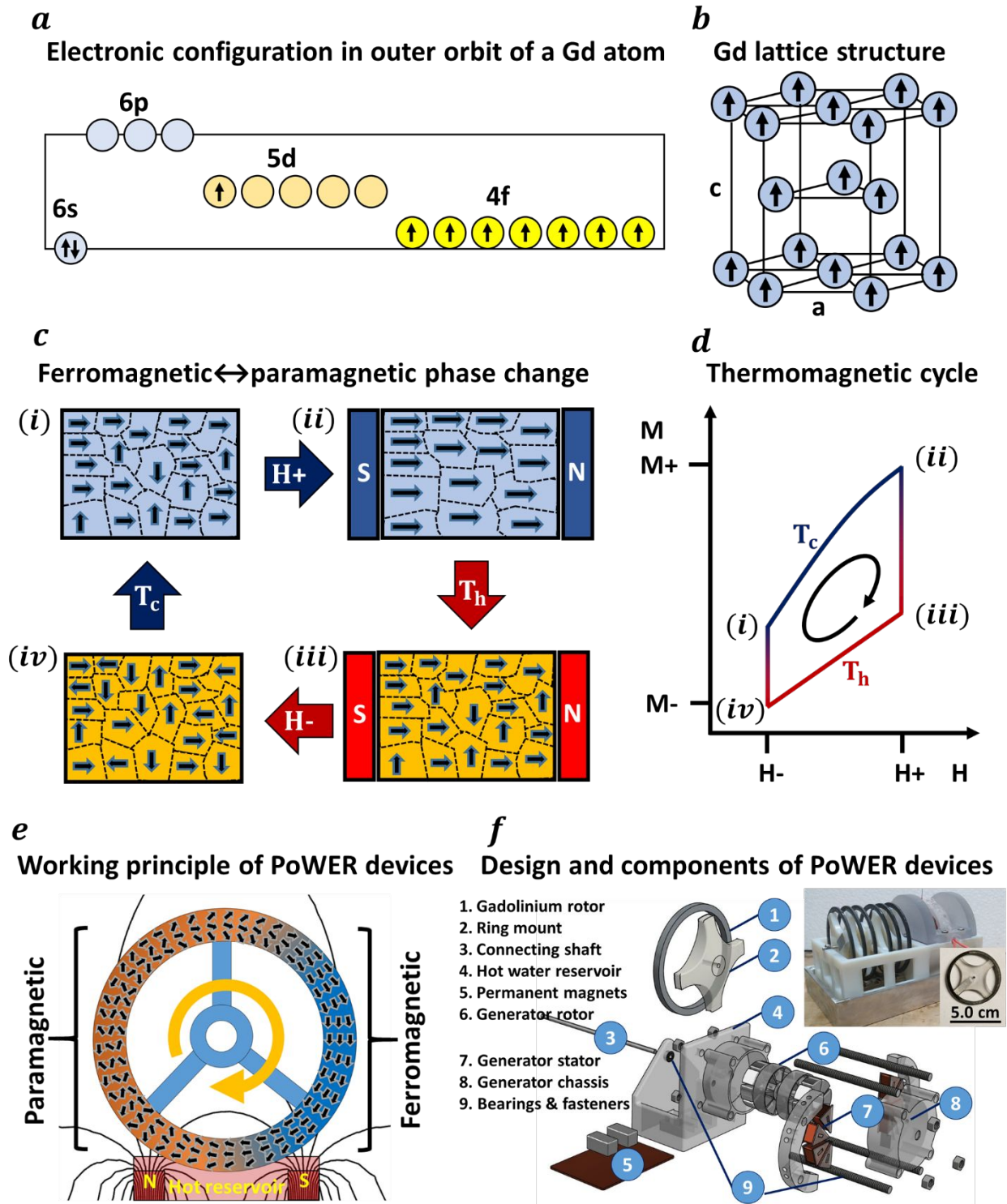
Fig. 1. Harvesting ultra-low grade thermal energy from surroundings. (a) The electronic configuration in the outer orbit of a neutral Gadolinium (Gd) atom. The seven unpaired electrons in the 4f subshell accounts for a large magnetic moment in Gd. (b) The hexagonal close-packed

(hcp) structure of Gd crystal. From spin reorientation temperature (-41°C) to Curie temperature (22°C), the magnetic moments are aligned along the hexagonal axis (c-direction). (c) The thermal energy harvesting utilizing thermomagnetic material that can be employed to obtain magnetic work. (d) The thermomagnetic cycle, where Gd sample undergoes the second-order paramagnetic↔ferromagnetic phase transformation in a cyclic manner. (e) The working principle of the proposed ultra-low grade thermal energy recovery mechanism, PoWER (Power from Waste Energy Recovery). Cyclic heating and cooling causes magnetic domains to orient and disorient, resulting in time-varying magnetization and an unbalanced magnetic torque on the rotor. (f) The design architecture and key components of the PoWER device. A prototype of the PoWER device with six rotors is shown in inset.
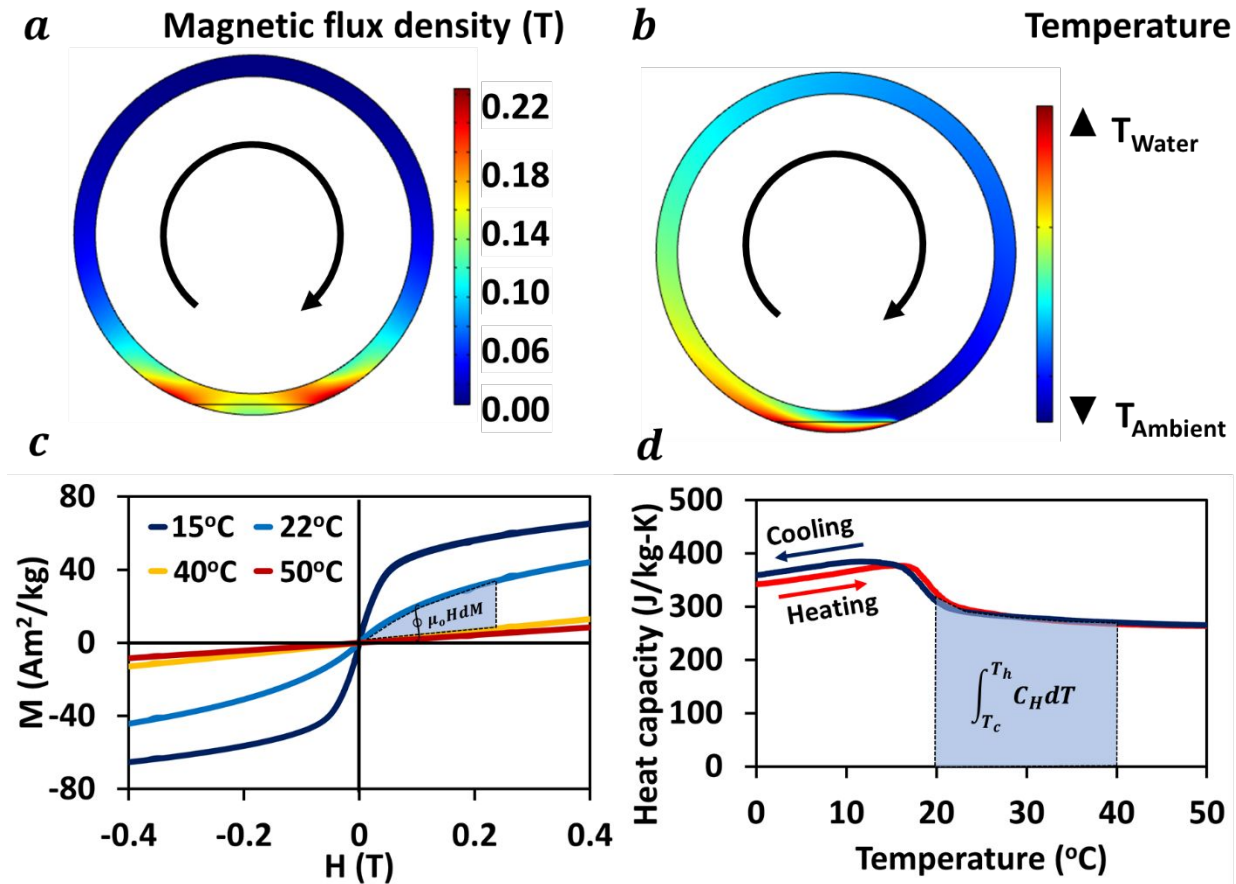
Fig. 2. Thermomagnetic cycle in the PoWER rotor. (a) The magnetic flux density distribution along the surface of the PoWER rotor. (b) The temperature contour showing the temperature distribution along the surface of the PoWER rotor. The actual temperature depends on the angular speed of the PoWER rotor. (c) Isothermal magnetization-magnetic field (M-H) curves of Gd. The shaded region illustrates the specific work. Isotherms are very close at high temperature, indicating minimal increase in specific work above 40°C. (b) Heat capacity versus temperature of Gd sample used in the PoWER devices. The shaded region indicates the heat flow during thermomagnetic cycle.
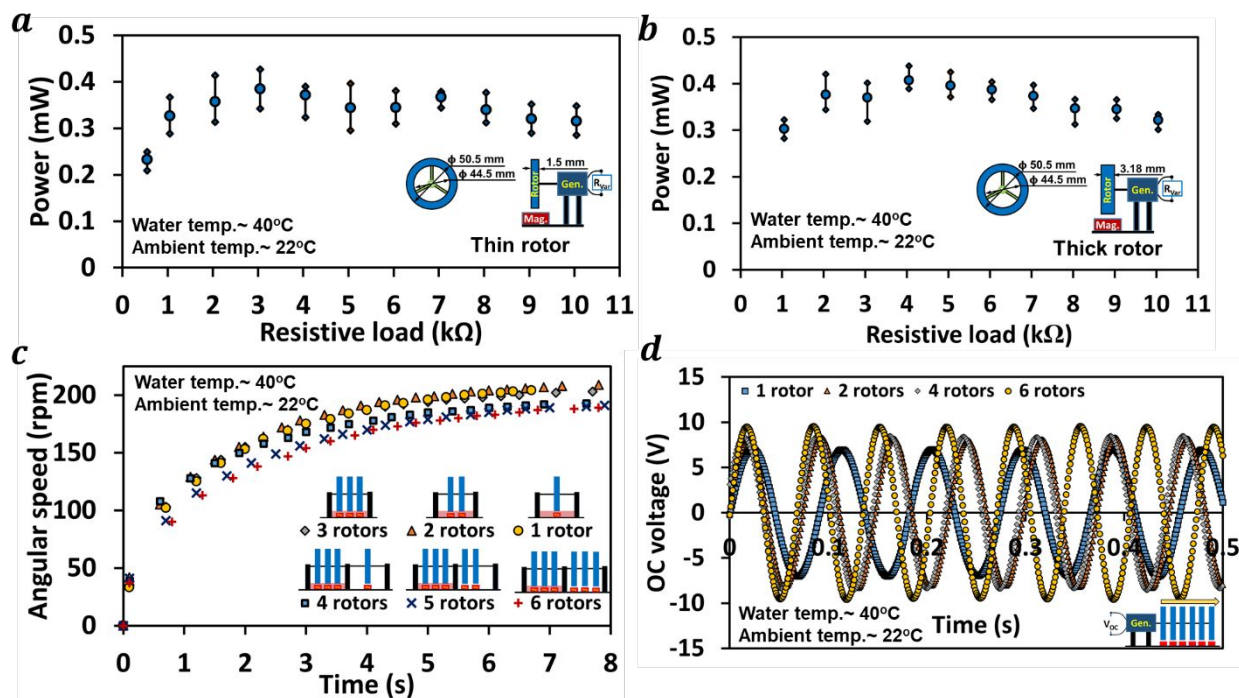
Fig. 3. Electrical power produced by PoWER devices as a function of resistive load at water temperature of 40°C and ambient temperature of 22°C. (a) The maximum, minimum, and average electrical power output of the PoWER device having thin rotor of dimension 50.5 mm (OD) × 44.5 (ID) × 1.5 mm (thickness). (b) The maximum, minimum, and average electrical power output of the PoWER device having thick rotor of dimension 50.5 mm (OD) × 44.5 (ID) × 3.18 mm (thickness). The thicker rotor (3.18 mm thickness) produces 6% higher power than the thinner one (1.5 mm thickness). (c) The angular speed progression of the PoWER rotors from the time it starts until it reaches the steady state. The number of rotors does not significantly affect the steady state angular speed and the rate of angular acceleration, indicating the thermomagnetic cycle of different rotors are mutually independent and the magnetic torque can be increased by multiplying the number of rotors. (d) Open circuit (OC) voltage obtained for different PoWER devices having one, two, four, and six rotors, respectively. OC voltage has frequency of 12.7 Hz, 13.1 Hz, 13.5 Hz, and 14.3 Hz, respectively, and amplitude above 1.0 V to minimize losses during rectification.
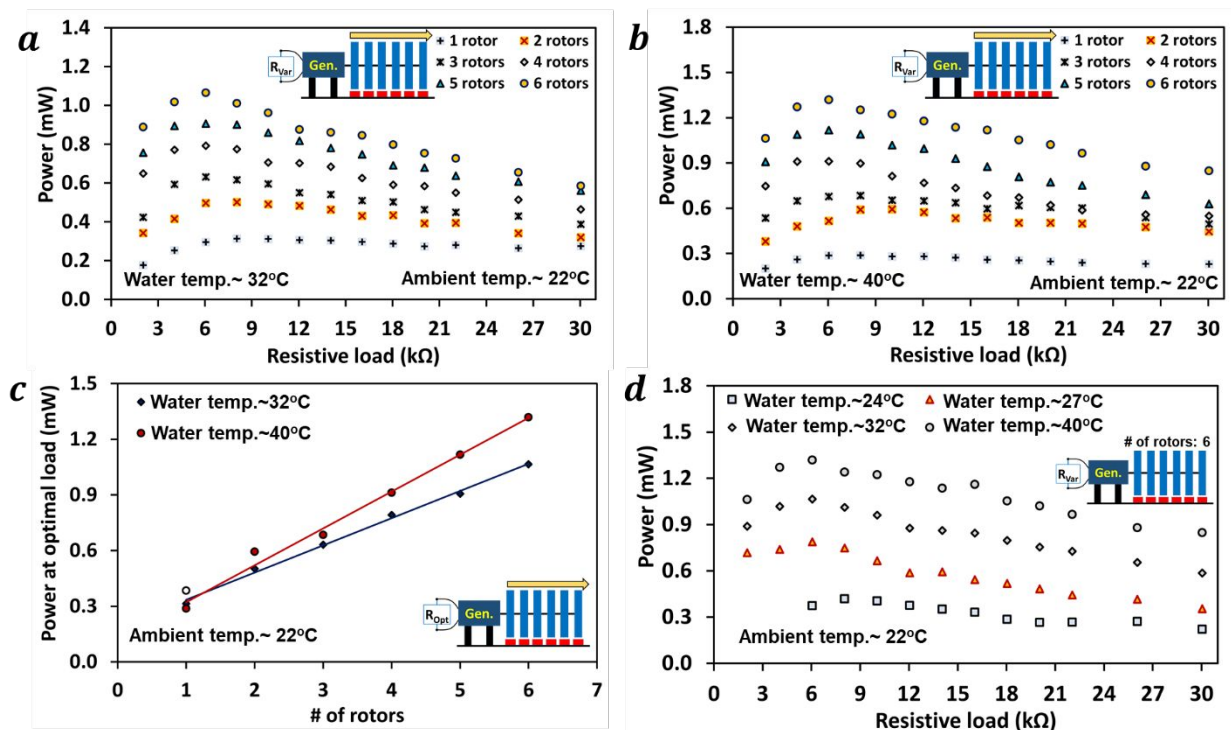
Fig. 4. Electrical power produced by PoWER devices having multiple rotors as a function of resistive load. (a) The average electrical power produced by the PoWER device having multiple rotors, connected simultaneously to a single generator shaft. At water temperature of 32°C, the electrical power at the optimal resistive load increases from 0.31 mW to 1.10 mW by increasing the number of rotors from one to six. (b) The average electrical power produced by the PoWER device having multiple rotors at 40°C. The electrical power at the optimal resistive load increases from 0.30 mW to 1.30 mW by increasing the number of rotors from one to six. (c) The optimal power of the PoWER devices versus number of rotors. Hollow circle shows the optimal power by the PoWER device with single rotor attached to small generator. Optimal power increases almost linearly with increase in the number of rotors, emphasizing the fact that the device is scalable and the power per unit volume of the device can be increased substantially by multiplying the number of rotors. (d) The average power of the PoWER device with six rotors at different hot-water temperature. The PoWER device produces optimal power of 0.42 mW at water temperature of 24°C (temperature difference of 2°C) and 0.79 mW at water temperature of 27°C (temperature difference of 5°C).
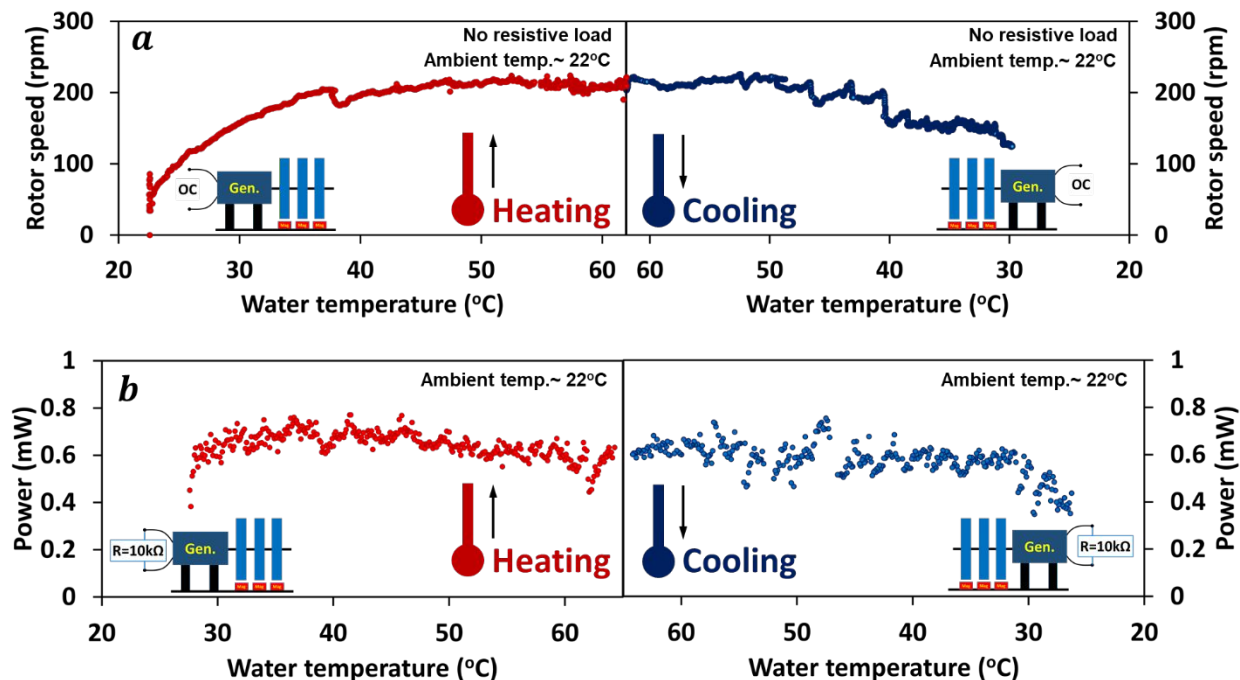
Fig. 5. Temperature sweep experiment for the PoWER device with three rotors. (a) Variation in rotor rpm with increase and decrease in water temperature. When water temperature is very low, rotor speeds up, but as water temperature rises above a threshold value, rotor achieves nearly a constant speed. (b) Variation in power output of the PoWER device with increase and decrease in water temperature. The electrical output first increases with increase in temperature, reaches a maximum value at 35-45°C, and then decreases slowly.
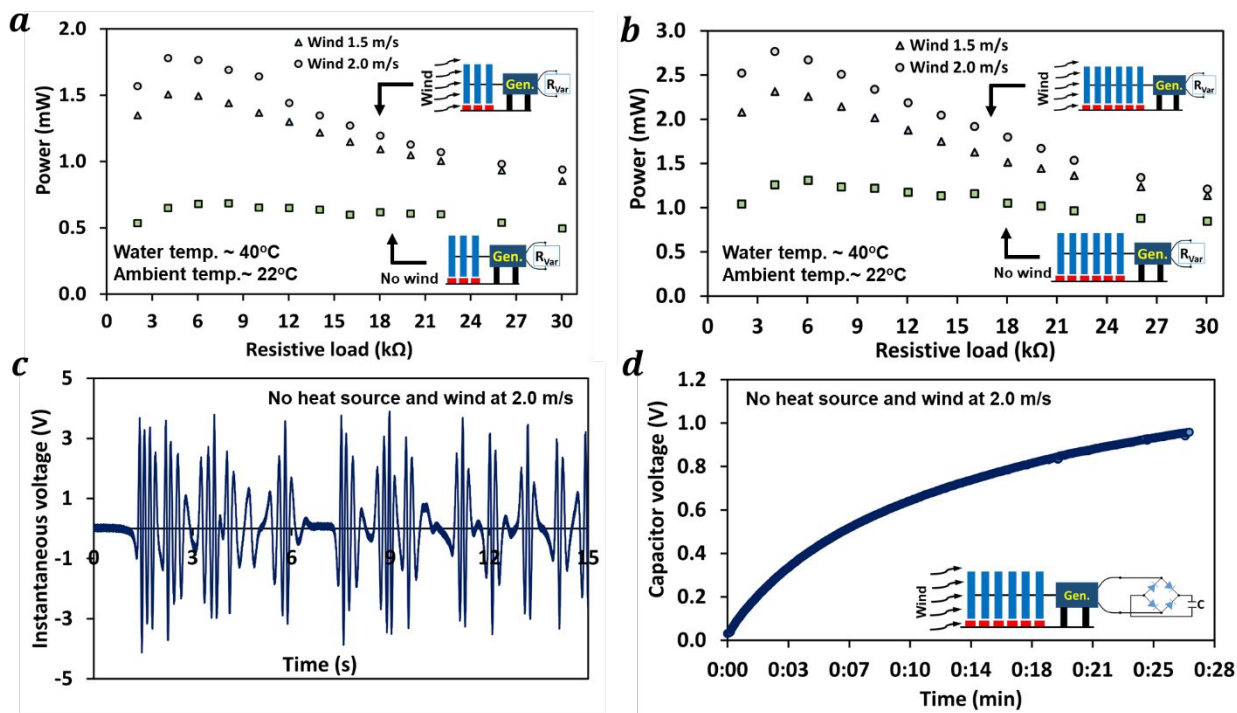
Fig. 6. Effect of wind (forced cooling) on the performance of PoWER devices. (a) Performance of the PoWER device with three rotors at wind speed of 1.5 m/s and 2.0 m/s. The optimal power of the PoWER device with three rotors increases from 0.69 mW in no wind conditions to 1.5 mW in a wind condition of 1.5 m/s and 1.8 mW in a wind condition of 2.0 m/s. (b) Performance of the PoWER device with six rotors at wind speed of 1.5 m/s and 2.0 m/s. The optimal power of a PoWER device with six rotors increases from 1.3 mW in no wind conditions to 2.3 mW under wind speed of 1.5 m/s and 2.8 mW under wind speed of 2.0 m/s. (c) Voltage generated by the PoWER device when there is no heat source but wind speed of 2.0 m/s. (d) The voltage across the two terminates of a 2.5 V 0.2 F capacitor being charged using the power produced by the PoWER device under no heat source and wind of 2.0 m/s.
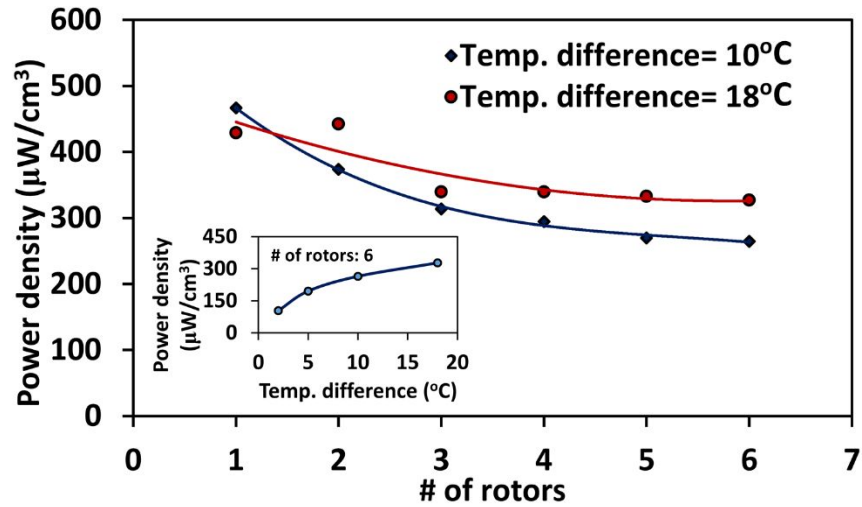
Fig.7. Power density (power per unit volume of Gd) demonstrated by PoWER devices having various number of rotors. Figure in the inset shows power density for the PoWER device with six rotors at different temperature difference.
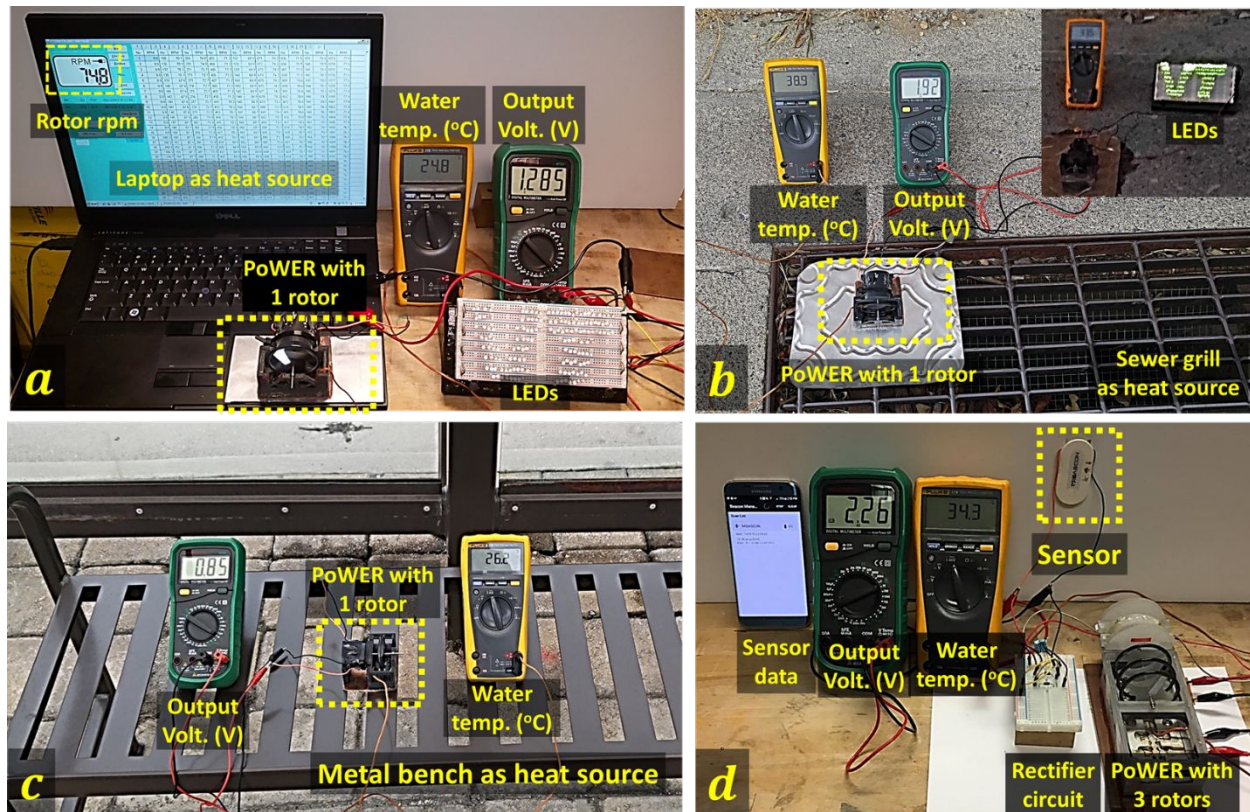
Fig. 8. Some real-world demonstrations. (a) A PoWER device with a single rotor kept on the surface of a laptop. Utilizing rejected heat from the laptop, the PoWER device can power several LEDs. (b) A PoWER device located on sewer grill. The PoWER device generates electricity using the steam coming out of sewage and drainage system. (c) A PoWER device with single rotor is kept on a metal bench exposed to sun light. PoWER device can operate under thermal gradient of just 1°C between the heat source and the ambient. (d) A MIDASCON sensor being powered by PoWER device. The sensor measures temperature, humidity, and acceleration and transmit the data wirelessly using Bluetooth.